Retrieval of Atmospheric Optical Depth Profiles from Downward-Looking High-Resolution O_2 A-Band Measurements: Optically Thin Conditions

QILONG MIN AND LEE C. HARRISON

Atmospheric Sciences Research Center, The University at Albany, State University of New York, Albany, New York

(Manuscript received 8 August 2003, in final form 1 April 2004)

ABSTRACT

A quasi-linear retrieval was developed to profile moderately thin atmospheres using a high-resolution O_2 A-band spectrometer. The retrieval is explicitly linear with respect to single scattering; the multiple-scattering contribution is treated as a perturbation. The properties of the linear inversion, examined using singular value decomposition of the kernel function, demonstrate the impacts of instrument specifications, such as resolution, out-of-band rejection, and signal-to-noise ratio, on information content. A system with 0.5 cm^{-1} resolution, signal-to-noise ratio of 100:1, and out-of-band floor of 10^{-3} has four independent pieces of information.

A fast radiative transfer model was developed to compute the multiple-scattering perturbation, in which multiple scattering is calculated at 16 different O_2 absorption depths to synthesize the O_2 A band. The linear system is then solved using Tikhonov's regularization with inequality constraints. Tests with synthetic data, including noise, of O_2 A-band retrievals illustrate that this algorithm is accurate and fast for retrieving aerosol profiles. The errors are less than 10% for the integrated total optical depth for the cases tested. It is shown that instruments with the needed performance are practical.

1. Introduction

Oxygen A-band (≈760 nm) remote sensing has been studied extensively for retrieval of surface pressure and cloud-top heights from satellite measurements (Mitchell and O'Brien 1987; Fischer and Grassl 1991; Fischer et al. 1991; O'Brien and Mitchell 1992). More recently, efforts have been made to use ground-based A-band measurements to infer photon pathlengths and to relate these to column properties (Harrison and Min 1997; Pfeilsticker et al. 1998; Veitel et al. 1998; Min and Harrison 1999; Portmann et al. 2001; Min et al. 2001; Min and Clothiaux 2003). All of these efforts have depended on limited information retrieval from the A band: effectively, little more than one eigenvector, though differently used.

In principle more information about the photon pathlength distribution can be inferred from high-resolution spectrometry of the A band (Min et al. 2004). High spectral resolution measurements may be capable of discriminating atmospheric scattering from surface scattering, and thus provide a better remote sensing technique for retrieving vertical aerosol profiles and clouds optical properties (Stephens and Heidinger 2000; Heidinger and Stephens 2000; Stephens et al. 2004 for detailed review).

Corresponding author address: Qilong Min, ASRC, The University at Albany, SUNY, 251 Fuller Road, Albany, NY 12203.
E-mail: min@asrc.cestm.albany.edu

The atmosphere appears very different in the A band than other wavelength regimes; on absorption-line centers in the A band the transmission to the ground is less than 10^{-30}. This is far less transmission than any measurement can observe, both for reasons of dynamic range in signal acquisition and out-of-band (OOB) rejection. However, we do not need extinctions anywhere near so extreme; by looking down into the atmosphere at strongly absorbing wavelengths (necessitating high resolution and good stray-light rejection) high-altitude scatterers appear bright and what lies below is invisible. In concept we can observe scattering from successively deeper layers by measuring at consecutively lower absorptions.

High-resolution (≈0.5 cm^{-1}) O_2 A-band instruments were proposed for the Cloudsat, Cloud-Aerosol Lidar and Infrared Pathfinder Satellite Observations (CALIPSO), and the Orbiting Carbon Observatory (OCO) missions; unfortunately, both Cloudsat and CALIPSO A-band instruments were ancillary measurements for active remote sensing efforts, and both were canceled due to difficulties with other portions of the satellite systems. Nonetheless, a substantial improvement in the understanding of O_2 A-band inversions and utility has been gained from the studies made for these satellites. A variety of practical goals seems possible given adequate instrument and inversion performance, such as measuring high-altitude cloud optical depths when low-level stratus is present, or cloud and aerosol optical

depths over high-albedo surfaces (e.g., snow); both are significant deficiencies in our current cloud and aerosol observations and climatologies. The Scanning Imaging Absorption Spectrometer for Atmospheric Chartography (SCIAMACHY) on the Environmental Satellite (*ENVISAT*) measures O_2 A band with a resolution of 0.48 nm. Recently, the OCO mission has been approved and a high-resolution instrument suite (O_2 A band and two CO_2 bands) will be launched in 2007. We would expect more high-resolution instruments in the future.

Here we develop a quasi-linear inversion algorithm for retrieving profiles of aerosol optical depth from downward-view spectroscopy from the top of the atmosphere (TOA). This algorithm permits nonlinear corrections suitable for the modest multiple scattering under conditions where the surface can still be seen. The method splits the retrieval into a linear problem, which can be considered as the single-scattering approximation, and then a multiple-scattering correction, which can be subtracted from radiances, to leave a single-scattering (linear) inversion. We show this formulation first, and then discuss the properties of the linear inversion based on the single-scattering approximation (the information content cannot be better than this), particularly the singular value decomposition (SVD) of the inversion kernels for various instrument performances (resolution, stray-light rejection, and signal-to-noise ratio) to demonstrate the consequences of instrument specification on potential retrievals.

2. Quasi-linear retrieval algorithm

a. Kernel functions

Extensive sensitivity studies show that the dominant contributions for observed radiance are due to the single- and/or lower-order scattering for small O_2 absorption optical thickness (k) and single scattering for large k, under optically thin conditions. Therefore, we split the radiance into two components and treat the multiple-scattering component as a perturbation using a fast-forward model to calculate it (more discussion later). In general, we have

$$I_{\text{ref}}(\lambda) = I^{\text{ss}}_{\text{ref}}(\lambda) + I^{\text{ms}}_{\text{ref}}(\lambda), \tag{1}$$

where ''ss'' and ''ms'' represent single-scattering and multiple-scattering, respectively.

For the single-scattering radiance, we have

$$\begin{aligned} I^{ss}(\mu, p) &= A_s\mu_0\frac{F}{\pi}\exp\left[-m\int_0^{p_0}\sigma_{\text{all}}(x)\,dx\right] + \int_0^{p_0}\frac{F}{4\pi\mu}\sigma(p)\omega(p)P(\mu_0, \mu, p)\exp\left[-m\int_0^{p_0}\sigma_{\text{all}}(x)\,dx\right] \\ &= A_s\mu_0\frac{F}{\pi}\exp\left[-m\int_0^{p_0}\sigma(x)\,dx\right]\exp\left[-m\int_0^{p_0}\sigma_{O_2}(x)\,dx\right] \\ &\quad + \int_0^{p_0}\frac{F}{4\pi\mu}\sigma(p)\omega(p)P(\mu_0, \mu, p)\exp\left[-m\int_0^{p}\sigma(x)\,dx\right]\exp\left[-m\int_0^{p}\sigma_{O_2}(x)\,dx\right], \end{aligned} \tag{2}$$

where A_s is the surface albedo; σ is the extinction coefficients of scatterers (aerosol and molecules) and absorptions (oxygen and ozone); ω is the single-scattering albedos of scatterers; P is the phase function of scatterers; p is the pressure of the atmosphere; m is the airmass factor; and μ and μ_0 are the cosine of scattering angle and cosine of solar zenith angle, respectively. The first term is the contribution by the surface reflection, and the second term is the contribution of scattering in the atmosphere. We further split O_2 absorption from other contributions to separate their contributions. If we define

$$\phi(p) = \frac{F}{4\pi\mu}\sigma(p)\omega(p)P(\mu_0, \mu, p)\exp\left[-m\int_0^{p}\sigma(x)\,dx\right]$$

$$T^{O_2}(p) = \exp\left[-m\int_0^{p}\sigma_{O_2}(x)\,dx\right], \tag{3}$$

when treating the surface reflection as one additional scattering layer, we have

$$I^{ss}(\mu, p) = \int_0^{p_0}\phi(p)T^{O_2}(p)\,dp. \tag{4}$$

The kernel function of the system, $T^{O_2}(p)$ is the transmittance of O_2 absorption. This yields an ill-conditioned first-order Fredholm equation. Without careful constraint unphysical solutions are likely. Here an obvious constraint is $\phi(p) \geq 0$. Further, if we define,

$$\frac{\partial\psi(p)}{\partial p} = \frac{F}{4\pi\mu}\sigma(p)\omega(p) \times P(\mu_0, \mu, p)\exp\left[-m\int_0^{p}\sigma(x)\,dx\right], \tag{5}$$

$\psi(p)$ can be viewed as the transmittance of the atmo-

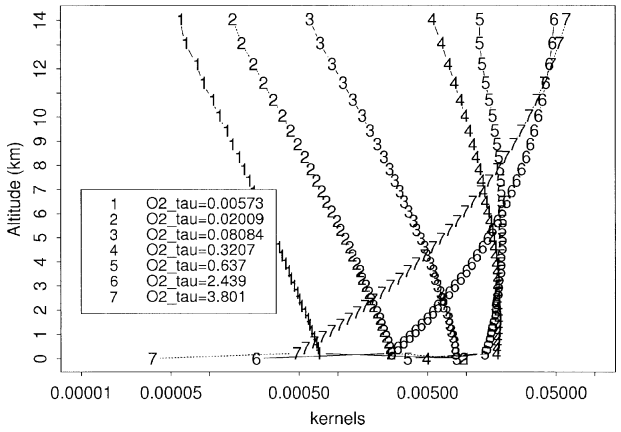

FIG. 1. The differential kernel functions of O_2 A band for various absorption depths.

sphere without O_2 absorption. It is positive and decreases monotonically from the TOA to the surface. Then by a partial integration, we have

$$I^{ss}(\mu, p) = A_s \mu_0 \frac{F}{\pi} \exp\left[-m \int_0^{p_0} \sigma(x)\, ds\right] T_M^{O_2} + \psi_0 T_0^{O_2} - \psi_M T_M^{O_2} - \int_0^{p_0} \psi \left(\frac{\partial T^{O_2}}{\partial p}\right) dp, \quad (6)$$

where ''0'' and ''M'' represent the top and bottom boundaries, respectively. We discretize the integration and have

$$I^{ss}(\mu, p) = \sum_i \psi_i \left(\frac{\partial T^{O_2}}{\partial p}\right)_i \quad \text{and}$$

$$\psi_0 \geq \psi_1 \geq \psi_2 \geq \cdots \geq \psi_M \geq 0, \quad (7)$$

where $(\partial T^{O_2}/\partial p)$ is the newly defined differential transmittance kernel function.

The introduction of this differential form is analogous to differential kernels common in longwave remote sensing, but we do not have a Planck function to differentiate analytically. Instead, this is an introduction of a partial integration. It is not evident a priori that this will be better behaved than the simple transmittance kernel; we will show that it is better from the conditioning parameters of SVD for the respective single-scattering kernels (see Fig. 3).

Figure 1 shows the differential kernel functions for various O_2 absorption depths (k). The deeper in the absorption line (larger in k) the higher altitude the maximum of the kernel function is located, and the less contribution comes from the surface layer (bottom layer). This kernel function provides us a qualitative explanation of the following important issue: the necessity of high-resolution spectrometry to ''see'' properties of the atmosphere not accessible otherwise.

b. Instrument impacts and information content

An important understanding that was gained as part of the development of Cloudsat and CALIPSO A-band instruments is that the information that might be inferred through an inversion process using measurements will be greatly influenced by the instrument performance. Figure 2 illustrates impacts of slit functions (resolutions and the OOB rejections) on the distributions of O_2 absorption depths. Other studies (Heidinger and Stephens 2000) considered resolution with the assumption of perfect stray-light rejection; these figures demonstrate that the information content of high-resolution absorption spectroscopy depends particularly on low stray-light contribution to the measurement, and that the OOB rejection criterion becomes more stringent as the resolution is improved (Harrison and Min 1997).

We use the SVD analysis on the differential–transmittance inversion kernels for various resolutions and OOB rejections to study the consequences of instrument specification on potential retrievals (Hansen 1998; Rodgers 2000). Figure 3 shows normalized singular values for a differential kernel function and a transmittance kernel function for two instrument resolutions of 1 (red line) and 0.5 cm^{-1} (blue lines) and four OOB rejections of 10^{-2}, 10^{-3}, 10^{-4}, and 10^{-5} (solid, dotted, dashed, and long-dashed lines, respectively). For the same instrument resolution and OOB rejection, the differential kernel function is more robust than the transmittance kernel function.

An important practical point is that if the instrument has inadequate OOB rejection, the real information content for inversion purposes is *improved* by degrading the resolution. A system with 0.5 cm^{-1} resolution, a signal-to-noise ratio of 100:1, and an OOB floor of 10^{-3} has four independent pieces of information.

Optimizing to get the maximum information from measurements is our major effort of developing retrieval algorithms. Before continuing we wish to stress that the needed instrument performance specifications are achievable. Min et al. (2004) show observations from a high-resolution spectrometer for both O_2 A band and water vapor band with a resolution of better than 0.5 cm^{-1} and an OOB rejection of 10^{-5}.

c. Tikhonov's regularization with inequality constraints

The differential transmittance kernel function [Eq. (7)], it is an ill-conditioned first-order Fredholm equation. All realistic solutions must have a monotonically decreasing aerosol transmittance with depth (after Rayleigh and absorption terms are removed). Here we use Tikhonov's regularization [known earlier as ''Twomey's method,'' see Hansen (1998) for a thorough overview and related methods] augmented with inequality constraints to retrieve the aerosol vertical profiles.

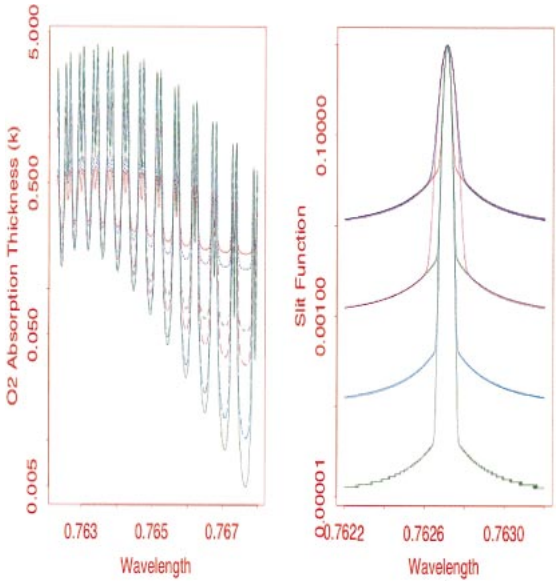

FIG. 2. (left) Oxygen A-band absorption depth spectra for (right) various extended slit functions.

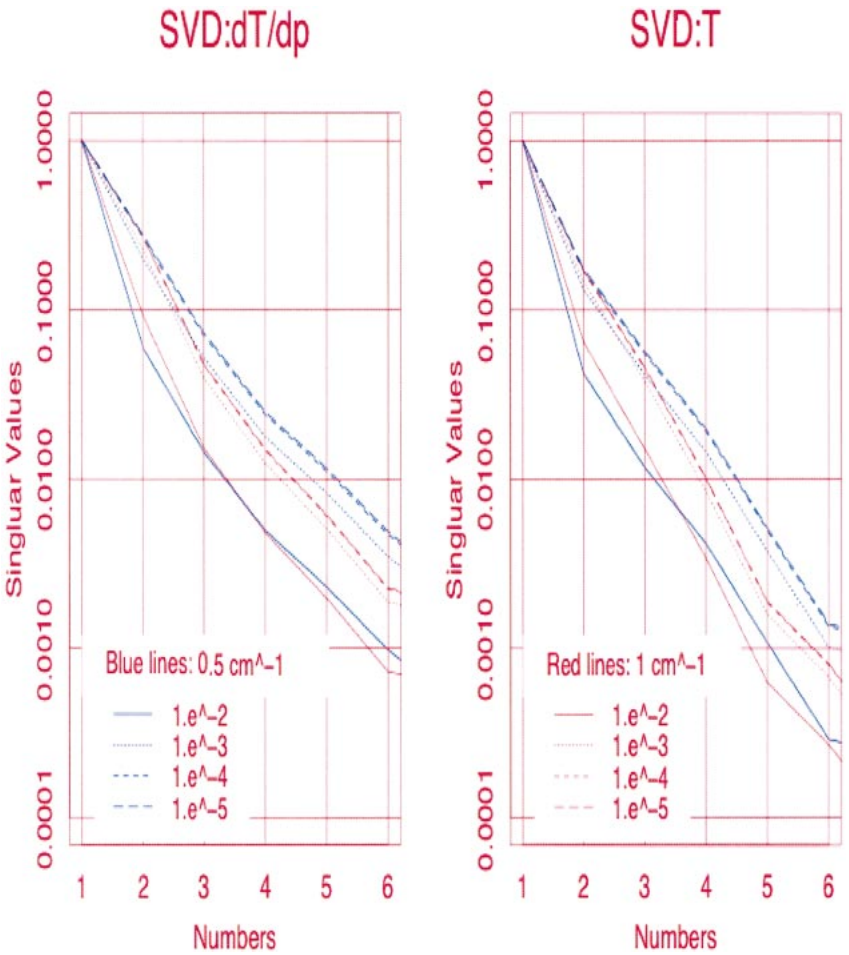

FIG. 3. The normalized singular values for both differential and transmittance kernel functions for different slit functions.

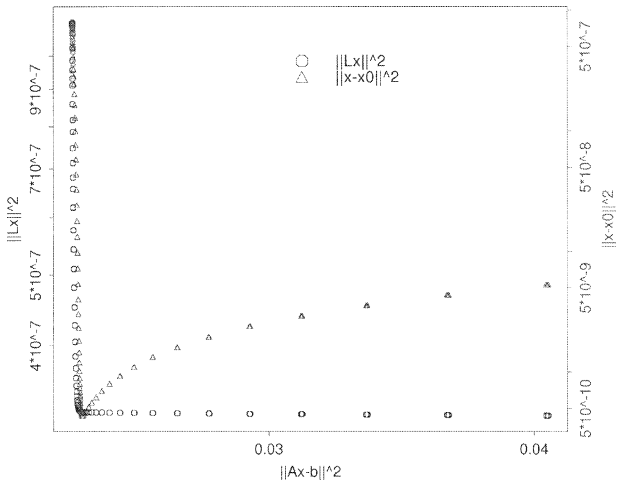

FIG. 4. The L curve of norm of $\mathbf{Ax} - \mathbf{b}$ vs $\mathbf{Lx}$ and the error between the true and retrieved solution.

Here

$$\min\{\|\mathbf{Ax} - \mathbf{b}\|_2^2 + \lambda^2\|\mathbf{Lx}\|_2^2\}$$
$$\text{subjected to} \quad \mathbf{Gx} \geq 0, \tag{8}$$

where $\mathbf{A}$ is our kernel matrix; $\mathbf{b}$ is the observation vector; $\mathbf{L}$ and $\mathbf{G}$ are the first derivative operators; and λ is a Lagrangian multiplier.

Basically, in a least squares sense, we minimize the forward model and observation with a regularization constraint (''smoothness'' constraint) of the solution. More importantly, such a solution is subject to an inequality constraint such that our ψ decreases monotonically.

To properly choose the Lagrangian multiplier or to find the optimal trade-off between the imposed smoothness and the residue error, we use the L-curve approach (Hansen 1998). In Fig. 4, the circles show the L curve, and the triangles show the error between true and retrieved solutions. The best solution is located at the corner L curve. In practice, λ is determined by the maximum curvature of the L curve or the best trade-off point,

$$\max\left[\frac{\eta'\rho'' - \rho'\eta''}{(\eta^2 + \rho^2)^{3/2}}\right], \tag{9}$$

where $\eta = \log(\|\mathbf{Ax} - \mathbf{b}\|_2^2)$, and $\rho = \log(\|\mathbf{Lx}\|_2^2)$. However, the maximum curvature may not be the optimal feature of the L curve for selecting the regularization parameter for some cases (Vogel 1996). Based on the trials with simulated data and noise, we use a value for λ that is twice that of the maximum curvature of the L curve.

d. A fast-forward radiative transfer (RT) model

For our quasi-linear retrieval, even though the multiple scattering is a small perturbation, we must calculate it and remove its contribution from our measurements. It is crucial to have a faster RT model to reduce computational cost, so that the algorithm can be used operationally. Most of the computational cost is spent to solve an RT equation for multiple scattering that, in general, depends on number of atmospheric layers and streams.

We can reduce the computation of the multiply scattered radiances because these fields are smoother, resulting in a photon pathlength distribution that is smooth. Taking advantage of the properties of photon pathlength distributions, we transform our problem from wavelength space to O_2 absorption optical thickness space (or k space). Using the existence of the Laplace transform for the gamma distribution (as used by Harrison and Min 1997; Min et al. 2004), we make only finite calculations for chosen k's (equivalent to k-distribution methods) to extrapolate and interpolate for all k's. This implicitly defines the photon pathlength distribution from a finite distribution of k's and then applies it to all wavelengths.

The following equations illustrate the steps for building a fast-forward RT model:

$$\begin{aligned} I &= I^{ss}(\lambda) + I^{ms}(\lambda) \\ &\approx I^{ss}[Z^h(p, t), P^h, \lambda] + I^{ms}[Z^h(p, t), P^h, \lambda] \\ &\approx I^{ss}[Z^h(p, t), P^h, \lambda] + I^{ms}[Z^h(p, t), P^l, \lambda] \\ &\approx I^{ss}[Z^h(p, t), P^h, \lambda] + I^{ms}[Z^l(p, t), P^l, \lambda] \\ &\approx I^{ss}[Z^h(p, t), P^h, \lambda] + I^{ms}\{F[Z^l(p, t), P^l, k(\lambda_i)]\}, \end{aligned} \tag{10}$$

where Z is all optical properties of the atmosphere as a function of pressure and temperature, P is the phase function of that layer, ss and ms stand for single and multiple (second-order and above) scattering, respectively. Here h and l represent higher and lower number of layers and streams, respectively, and F is the extrapolation and/or interpolation function from finite $k(\lambda_i)$, which can be written as $F[k(\lambda_i)] = \Sigma_{j=1}^{n}[A_j/(k - \alpha_j)^{\beta_{j+1}}]$. Thus the pathlength distribution is a summation of n gamma distributions. For the example below, we use two gamma distributions, which are defined by 16 k values at both ends of the O_2 A band.

Figure 5 shows differences between the bench model and the fast model for clear-sky conditions. The bench model is set up by 40 atmospheric layers and 32 streams, while the fast model is set up with 10 layers and 16 streams and only computes at 16 k values from 0.001 to 60. Both simulated observations are convolved by slit function of 0.5 cm^{-1} full-width half-maximum (FWHM) with the OOB rejection of 10^{-4}. For the clear-sky case the difference is less than 0.2% because the contribution of single scattering is dominant. The difference, shown in the figure, is mainly caused by the temperature dependence of O_2 absorption coefficients from line to line. If we only use one absorption line,

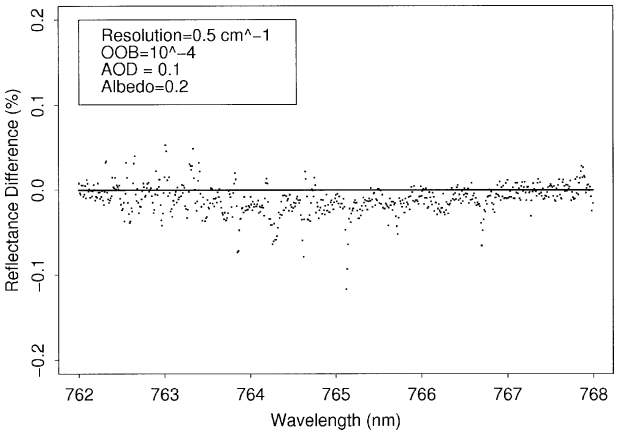

FIG. 5. Differences between the bench model and fast model for a clear-sky test case.

the difference will be reduced to less than 0.05%. The fast-forward model is more than 100 times faster than the standard radiation model that requires thousands of calculations in wavelength space.

3. Results

For all the test cases, the simulated measurements are calculated for an assumed instrument with resolution of 0.5 cm^{-1} and the OOB rejection of 10^{-4}. The simulated system will sample the spectrum between 762 and 768 nm with three pixels per FWHM. We also added white noise to the signal with a signal-to-noise ratio of 100. We use the Air Force Geophysics Laboratory (AFGL) atmospheric constituent profile for midlatitude summer and a dark surface. Total aerosol optical depth and vertical distribution are different for the following three cases, with the same single-scattering albedo and asymmetry factor of 0.95 and 0.75, respectively.

First we discuss a typical background aerosol case with total optical depth of 0.05 at 760 nm (see Fig. 7 for aerosol vertical profile). The left plot of Fig. 6 shows the integrated total optical depth from TOA down to the corresponding layer, including aerosol, Rayleigh scattering, and ozone. The number, *T*, and *G* represent the number of iterations, and the true and initial guess of profiles for the test case, respectively. The right plot shows the percentage differences after various iterations. After five iterations, the solution converged to within 5% of the true profile for altitudes below 8 km, where most aerosol and molecular scatterers exist. The total optical depth, which is primarily determined by the lowest-absorption pixels, however, agrees with the true optical depth to 2%. We have tested the sensitivity of final results to the initial-guess profile by using various initial-guess profiles. The final result converges very well to the true profile and is insensitive to the initial guess.

Figure 7 shows the extinction profiles of aerosol: true and final (fifth iteration). The differences between two profiles are less than 20%. This example shows a ''sharp'' aerosol profile to test the impact of the regularization. Most of the differences seen from the plot are the result of the smoothed retrieval.

Figure 8 shows a case of heavy aerosol loading with a total aerosol optical depth of 0.2 at 760 nm, but still with in our limit for ''optically thin.'' Similarly to case 1, after five iterations the solution converged to the true profile within 5% for altitudes below 8 km.

Sometimes the altitude of maximum of aerosol loading is above the surface, for example, volcanic or smoke plumes. This yields more challenging situations, which

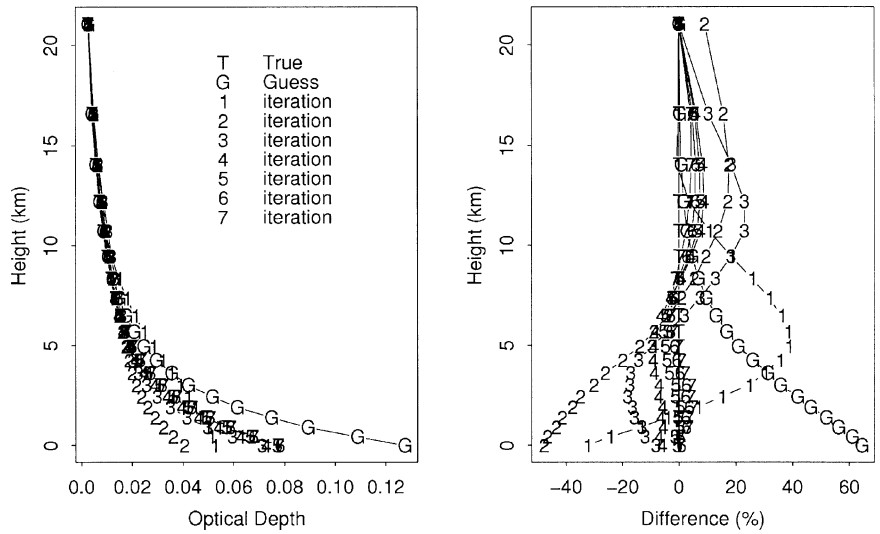

FIG. 6. Vertical profiles of integrated total optical depth from TOA and differences for various iterations. Total aerosol optical for this case is 0.05.

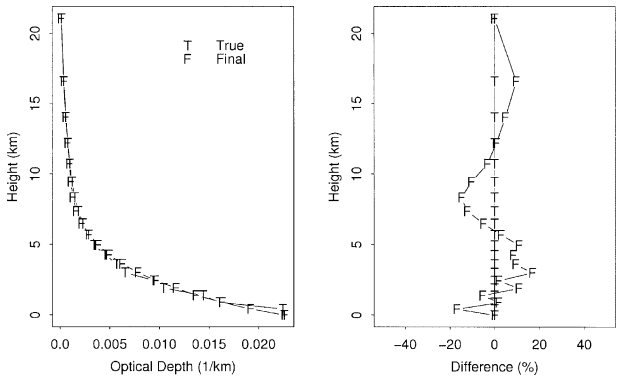

FIG. 7. Vertical extinction profiles of aerosol and differences between the true and retrieved solution. Total aerosol optical for this case is 0.05.

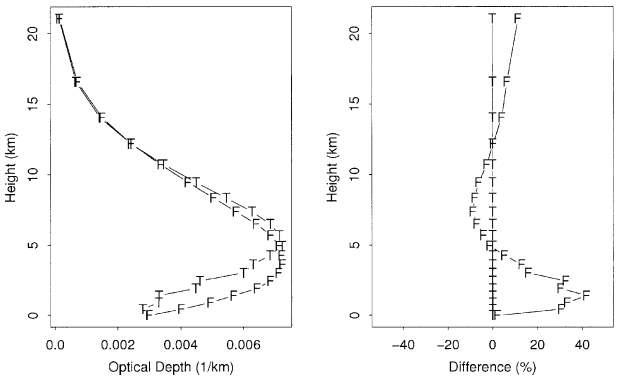

FIG. 9. Vertical extinction profiles of aerosol and differences between the true and retrieved solution. Total aerosol optical for this case is 0.05 with the maximum of aerosol optical depth at 5 km.

requires substantially higher O_2 absorption to resolve (see the kernel function in Fig. 1). We simulated this situation by assuming the maximum aerosol optical depth at 5 km with total aerosol optical depth of 0.05. Figure 9 shows the true and retrieved vertical extinction profiles of aerosol. After five iterations, the final result converges, but the maximum altitude is about 1 km lower than that of the true profile. The fractional difference is quite large in the region below the maximum altitude, even though the total optical depth agrees with 2%. The reasons the retrieved vertical distribution is biased toward a lower altitude are twofold: 1) the linear (single scattering) inversion cannot well resolve high-altitude scatters due to the limited resolving power for this chosen simulated instrument, and 2) the underestimated high-altitude scattering then is automatically amplified by an underestimation of the multiple-scattering correction.

The cases we selected are arbitrary and are not fully realistic. In reality, we do not have a priori knowledge of aerosol single-scattering albedos and phase functions, these must be assumed. The uncertainties of aerosol single-scattering properties will result in an error in profile of aerosol optical depths through correction of multiple scattering and conversion from transmittance function (ψ) to optical depth profile, even though the transmittance function is inverted from a linear system. Changes in a single-scattering albedo of 0.03 and in a phase function of 4% will result in uncertainties of 3.8% and 2.6% in total optical depth, respectively. In this paper we have assumed that the surface albedo is known and test cases used zero. For operational retrievals using this algorithm the surface albedo is formally an external input, as it is for many other optical retrievals (King et al. 1999 and reference therein). In principle the O_2 A-band observations can invert the surface albedo as an

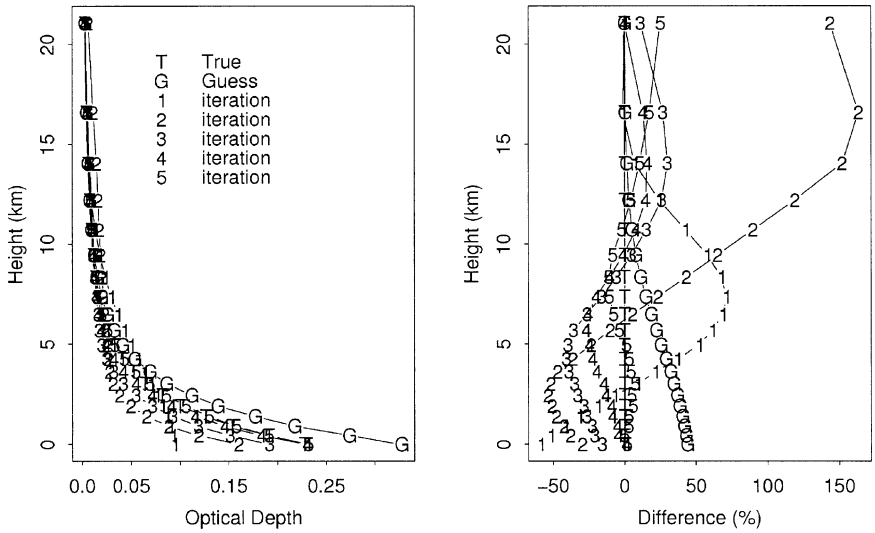

FIG. 8. Vertical profiles of integrated total optical depth from TOA and differences for various iterations. Total aerosol optical for this case is 0.20 with an increasing aerosol optical depth to the surface.

independent parameter, but sensitivity studies not fully discussed here show that this requires very demanding *k* values and accuracy of instrument observing functions to do so in the general case. Simultaneous retrieval of surface albedo and aerosol optical profile and issues of surface albedo on retrievals will be addressed in a following study.

4. Inequality constraints

In all the examples shown above, the results are a least square (LS) solution without the subsequent Nonnegative least squares (NNLS) constrained solution. The first step of the NNLS yields a least squares (LS) solution, and further work stops if the conditions are met. One advantageous consequence of this is that the SVD description of the information content of the inversion is appropriate, at least for the local domain around the final solution. (The NNLS cannot be described as a linear operator or ''regularization'' operating solely on the kernel function, since it depends on the observation vector, and hence we cannot study the SVD of NNLS inversion.) The use of NNLS may be necessary to prevent iterations for multiple-scattering corrections from diverging aphysically.

In the event that the ''final'' solution requires NNLS constraint, one of two situations is obtained: if the distance from this solution and the unconstrained LS solution is within the range predicted from the covariance matrix of the regularized kernel, then it can be viewed as acceptable and a consequence of ''ordinary'' noise propagation. If, however, this distance is significantly larger, it is evidence of inversion failure, and this can be tested for each result. The failure could occur for many reasons, but incorrect transmission kernel values (meaning an incorrect instrument performance characterization) would likely present themselves this way, as would serious errors in assumed ground albedo or aerosol optical properties.

5. Summary

We have developed a quasi-linear retrieval algorithm for moderately thin atmospheres to study issues of nadir-viewing high-resolution O_2 A-band remote sensing information content. This algorithm can be applied to many aerosol optical depth cases. The information that may be inferred is greatly influenced by the capability of the A-band spectrometer providing the measurements. Based on a single-scattering approximation, we investigate the issue of information content in terms of a linear retrieval as a function of two important instrument specifications: resolution and OOB rejection. A system with 0.5 cm^{-1} resolution, a signal-to-noise ratio of 100:1, and an out-of-band floor of 10^{-3} has four independent pieces of information. Further, we developed an accurate and fast radiative transfer model to correct the multiple scattering. We solved the linear system using Tikhonov's regularization with inequality constraints. We show that useful retrievals are possible for an instrument with 0.5 cm^{-1} provided that OOB rejection is adequate, and instruments with this performance are practical.

Acknowledgments. This research was supported by the National Aeronautics and Space Administration under Jet Propulsion Laboratory Contract 1207919.

REFERENCES

Fischer, J., and H. Grassl, 1991: Detection of cloud-top height from backscattered radiances within the oxygen A band. Part I: Theoretical study. *J. Appl. Meteor.,* **30,** 1245–1259.

——, W. Cordes, A. Schmitz-Peiffer, W. Renger, and P. Morel, 1991: Detection of cloud-top height from backscattered radiances within the oxygen A band. Part II: Measurements. *J. Appl. Meteor.,* **30,** 1260–1267.

Hansen, P. C., 1998: *Rank-Deficient and Discrete Ill-Posed Problems: Numerical Aspects of Linear Inversion.* SIAM, 247 pp.

Harrison, L., and Q.-L. Min, 1997: Photon pathlength distributions in cloudy atmospheres from ground-based high-resolution O_2 A-band spectroscopy. *IRS'96: Current Problems in Atmospheric Radiation,* W. L. Smith and K. Stamnes, Eds., Deepak Publishers, 594–597.

Heidinger, A., and G. L. Stephens, 2000: Molecular line absorption in a scattering atmosphere. Part II: Retrieval of particle properties. *J. Atmos. Sci.,* **57,** 1615–1634.

King, M. D., Y. J. Kaufman, D. Tanre, and T. Nakajima, 1999: Remote sensing of tropospheric aerosols from space: Past, present and future. *Bull. Amer. Meteor. Soc.,* **80,** 2229–2259.

Min, Q.-L., and L. C. Harrison, 1999: Joint statistics of photon pathlength and cloud optical depth. *Geophys. Res. Lett.,* **26,** 1425–1428.

——, and E. Clothiaux, 2003: Photon pathlength distribution inferred from the RSS at the ARM SGP site, ARM, 2001. *J. Geophys. Res.,* **108**, 4465, doi:10.1029/2002JD002963.

——, ——, and E. Clothiaux, 2001: Joint statistics of photon pathlength and cloud optical depth: Case studies. *J. Geophys. Res.,* **106,** 7375–7386.

——, L. C. Harrison, P. Kierdron, J. Berndt, and E. Joseph, 2004: A high-resolution oxygen A-band and water vapor band spectrometer. *J. Geophys. Res.,* **109**, D02202, doi:10.1029/2003JD003540.

Mitchell, R. M., and D. M. O'Brien, 1987: Error estimates for passive satellite measurement of surface pressure using absorption in the A band of oxygen. *J. Atmos. Sci.,* **44,** 1981–1990.

O'Brien, D. M., and R. M. Mitchell, 1992: Error estimates for retrieval of cloud top pressure using absorption in the A band of oxygen. *J. Appl. Meteor.,* **31,** 1179–1192.

Pfeilsticker, K., F. Erle, H. Veitel, and U. Platt, 1998: First geometrical pathlengths probability density function derivation of the skylight from spectroscopically highly resolving oxygen A-band observations. 1. Measurement technique, atmospheric observations and model calculations. *J. Geophys. Res.,* **103,** 11 483–11 504.

Portmann, R. W., S. Solomon, R. W. Sanders, and J. S. Danel, 2001: Cloud modulation of zenith sky oxygen path lengths over Boulder, Colorado: Measurements versus model. *J. Geophys. Res.,* **106,** 1139–1155.

Rodgers, C. D., 2000: *Inverse Methods for Atmospheric Sounding: Theory and Practice.* World Scientific, 238 pp.

Stephens, G. L., and A. Heidinger, 2000: Molecular line absorption in a scattering atmosphere. Part I: Theory. *J. Atmos. Sci.,* **57,** 1599–1614.

——, ——, and P. Gabriel, 2004: Photon paths and cloud heterogeneity: Toward an observational strategy for assessing the effects of 3D geometry on radiative transfer. *Three-Dimensional*

Radiative Transfer for Cloudy Atmospheres, X. Marshak and X. Davis, Eds., Springer-Verlag, in press.
Veitel, H., O. Funk, C. Kruz, U. Platt, and K. Pfeilsticker, 1998: Geometrical path length probability density functions of the sky-light transmitted by midlatitude cloudy skies: Some case studies. *Geophys. Res. Lett.*, **25,** 3355–3358.
Vogel, C. R., 1996: Non-convergence of the L-curve regularization parameter selection method. *Inverse Problem*, **12,** 535–547.